



HAL
open science

Imprints of Ocean Chaotic Intrinsic Variability on Bottom Pressure and Implications for Data and Model Analyses

Mengnan Zhao, Rui M. Ponte, Thierry Penduff, Sally Close, William Llovel, Jean-Marc Molines

► **To cite this version:**

Mengnan Zhao, Rui M. Ponte, Thierry Penduff, Sally Close, William Llovel, et al.. Imprints of Ocean Chaotic Intrinsic Variability on Bottom Pressure and Implications for Data and Model Analyses. *Geophysical Research Letters*, 2021, 48, 10.1029/2021GL096341 . insu-03683243

HAL Id: insu-03683243

<https://insu.hal.science/insu-03683243>

Submitted on 19 Aug 2022

HAL is a multi-disciplinary open access archive for the deposit and dissemination of scientific research documents, whether they are published or not. The documents may come from teaching and research institutions in France or abroad, or from public or private research centers.

L'archive ouverte pluridisciplinaire **HAL**, est destinée au dépôt et à la diffusion de documents scientifiques de niveau recherche, publiés ou non, émanant des établissements d'enseignement et de recherche français ou étrangers, des laboratoires publics ou privés.

Copyright

Geophysical Research Letters[®]

RESEARCH LETTER

10.1029/2021GL096341

Key Points:

- The imprint on bottom pressure of ocean chaotic intrinsic variability is explored using a large ensemble of simulations
- This random imprint is substantial in many regions, and exceeds the atmospherically driven variability in eddy-rich regions
- Chaotic intrinsic variations are important on spatial scales larger than mesoscale for seasonal and shorter timescales

Correspondence to:






M. Zhao,
mzhao@aer.com

Citation:

Zhao, M., Ponte, R. M., Penduff, T., Close, S., Llovel, W., & Molines, J.-M. (2021). Imprints of ocean chaotic intrinsic variability on bottom pressure and implications for data and model analyses. *Geophysical Research Letters*, 48, e2021GL096341. <https://doi.org/10.1029/2021GL096341>

Received 27 SEP 2021
Accepted 19 NOV 2021

Imprints of Ocean Chaotic Intrinsic Variability on Bottom Pressure and Implications for Data and Model Analyses

Mengnan Zhao¹ , Rui M. Ponte¹ , Thierry Penduff² , Sally Close³, William Llovel³ , and Jean-Marc Molines² 

¹Atmospheric and Environmental Research, Inc., Lexington, MA, USA, ²CNRS, IRD, Grenoble-INP, Institut des Géosciences de L'Environnement (IGE), Université Grenoble Alpes, Grenoble, France, ³Laboratoire D'Océanographie Physique et Spatiale (LOPS), University of Brest/IFREMER/IRD/CNRS, Brest, France

Abstract Variations in ocean bottom pressure are important for understanding ocean circulation and climate. While most studies have focused on atmospherically driven variability, here we use eddy-permitting large ensemble simulation output from the Oceanic Chaos–ImPacts, strUcture, predicTability (OCCIPUT) project to isolate chaotic intrinsic variability generated by nonlinear oceanic processes. Analyzing separately the mean seasonal cycle and remainder variability in intra-annual (60–365 days) and subseasonal (2–60 days) bands, we find intrinsic variations larger than atmospherically driven ones over eddy-active regions across all timescales, particularly in the intra-annual range, where intrinsic variations dominate in almost 25% of the oceans. At scales larger than mesoscale, intrinsic variability is still considerable, supporting the process of energy inverse cascade toward lower frequency and larger scales. Results highlight the importance of intrinsic variability over a range of spatiotemporal scales and provide new insights on the interpretation of GRACE-like observations and their de-aliasing procedures.

Plain Language Summary Variations in ocean bottom pressure reflect ocean mass redistribution and surface freshwater fluxes. The changes in ocean bottom pressure can be attributed to atmospherically driven signals and an oceanic intrinsic component, which is generated by the ocean itself and shows random and chaotic characteristics. While the former has been relatively well understood, the latter is less studied but important in interpreting bottom pressure measurements and model simulations. In this work, we use a large ensemble of global ocean/sea-ice model simulations from the Oceanic Chaos–ImPacts, strUcture, predicTability (OCCIPUT) project to isolate the intrinsic variations of ocean bottom pressure on subseasonal (periods <60 days) and intra-annual (period of 60 days–1 year) bands, as well as the mean seasonal cycle. Our results reveal substantial intrinsic variations at all timescales over regions with active mesoscale eddies, where intrinsic variations can be more important than atmospherically driven ones. Over intra-annual range, almost a quarter of the ocean shows stronger intrinsic variability. Considerable intrinsic variability is also found at scales larger than mesoscale, suggesting energy transfers from mesoscale to larger scales. Our work suggests the need for taking the intrinsic component into account when interpreting bottom pressure observations and model outputs.

1. Introduction

Ocean bottom pressure (p_b) variability reflects changes in mass of the water column arising from freshwater fluxes at the ocean boundaries and horizontal mass redistribution by the ocean circulation (e.g., Hughes et al., 2018; Johnson & Chambers, 2013; Landerer et al., 2015). Variations in p_b also provide information on manometric and barystatic sea level (Gregory et al., 2019), helping in the interpretation of altimetry data (e.g., Piecuch et al., 2013; Ponte, 1999). Knowledge of p_b and its dynamics is of great importance to better understand global ocean mass variations, circulation patterns, and freshwater and heat budgets.

Many past studies implicitly assume that p_b variations, especially at spatial scales larger than mesoscale and on monthly and longer timescales, are a direct response to atmospheric forcing (e.g., Androsov et al., 2020; Carrère & Lyard, 2003; Ponte, 1999; Ponte & Piecuch, 2014). However, in addition to this forced variability (p_b^f hereafter), there is the possibility of having chaotic intrinsic p_b variability (p_b^i hereafter) arising from non-linear ocean processes, as seen for example, in the observational analyses of Fu (2007) and Hughes et al. (2016). Although associated with mesoscale and smaller scale dynamics, p_b^i variability on larger spatial and longer temporal scales

can also result through nonlinear interactions (e.g., Arbic et al., 2012; Charney, 1971; Scott & Arbic, 2007; Venaille et al., 2011). In fact, the importance of such chaotic intrinsic variability has been found in sea level (e.g., Close et al., 2021; Llovel et al., 2018; Penduff et al., 2011, 2014, 2019; Sérazin et al., 2015) and other dynamical variables (e.g., Cravatte et al., 2020; Leroux et al., 2018; Penduff et al., 2018), but its impact on p_b remains to be studied in detail.

Characterizing the chaotic intrinsic component in p_b is a first step toward understanding its role in the large-scale variability of circulation and sea level. Basic knowledge of p_b^i is important when comparing and interpreting p_b variability in non-eddy-resolving numerical models and in the large-scale p_b measurements returned from the Gravity Recovery and Climate Experiment (GRACE) and the follow-on (GRACE-FO) missions. Indeed, intrinsic variability is strongly underestimated in non-eddy ocean models (Grégorio et al., 2015; Penduff et al., 2011) and entangled with forced signals in observations. In addition, GRACE aliasing errors, emerging from p_b variations at periods shorter than twice the mapping interval, could be better evaluated with knowledge of p_b^i variations. Usually modeled and then removed from the GRACE measurements (e.g., Dobslaw et al., 2016; Schindelegger et al., 2021; Seo et al., 2008), corrections based on models that inadequately represent p_b^i (e.g., Quinn & Ponte, 2011; Schindelegger et al., 2021) could degrade GRACE data quality. A more accurate representation of aliasing errors is still a crucial part in GRACE data processing.

Motivated by the lack of knowledge on the importance of p_b^i , in this study we take advantage of the eddy-permitting large ensemble of ocean/sea-ice simulations from the OceaniC Chaos–ImPacts, strUcture, predicTability (OCCIPUT) project (Bessières et al., 2017; Penduff et al., 2014) to isolate p_b chaotic intrinsic components from those driven by atmospheric external forcing. Aside from examining the mean seasonal cycle, we focus on two frequency bands: subseasonal (<60 days) and intra-annual (60 days–1 year). The subseasonal band corresponds to periods that are nominally aliased in GRACE and GRACE-FO missions. Examining p_b^i at seasonal and intra-annual timescales provides insight on its impacts on low frequency p_b . Interannual and longer variations are discussed in Carret et al. (2021).

This paper is structured as follows. In Section 2, the primary output used in this study from the OCCIPUT Large Ensemble is introduced. Section 3 provides details of the calculation of p_b^f and p_b^i from the OCCIPUT Large Ensemble. Section 4 describes characteristics of p_b^i over various frequency bands and examines them in the context of p_b variability from measurements and climate models. We summarize and discuss our findings in Section 5.

2. The OCCIPUT Large Ensemble Simulation

The main output used in this study are the global daily p_b fields generated by the OCCIPUT Large Ensemble (<https://meom-group.github.io/projects/occiput/>). The OCCIPUT Large Ensemble provides NEMO-based ocean/sea-ice hindcasts over 1960–2015. The simulations are eddy permitting, with a nominal $\sim 1/4^\circ$ horizontal resolution. The Large Ensemble consists of 50 members, each member distinguished by perturbations in initial conditions based on a common 21-year spin-up (Leroux et al., 2018; Penduff et al., 2014, 2019). The 50 members are driven by the same realistic 6-hourly atmospheric forcing [Drakkar Forcing set DFS 5.2, Dussin et al. (2016)] derived from atmospheric reanalyses.

Here we analyze p_b output from 1995 to 2015. The impact of model drift is accounted for by removing the linear trend of these 21-year p_b records for each grid point and individual ensemble member. All calculations in this study are based on the bottom pressure anomalies (p_b^i hereafter) resulting from the detrended time series.

We acknowledge that model drift and geophysical trends may not be linear. For example, in some studies, the Locally Weighted Scatterplot Smoothing (LOESS) filter was applied to remove signals with long periods for each ensemble member (e.g., Bessières et al., 2017; Close et al., 2021; Leroux et al., 2018). For a few test examples, we compared residuals after de-drifting using LOESS filter and linear detrending and found no effective differences (not shown). Other de-drifting methods include removing the linear trend from a run driven by climatological forcing (e.g., Llovel et al., 2018; Penduff et al., 2019). Taking into consideration the computational speed and the available output, in this study we use the linear detrending method to minimize influence from model drift. In any case, we focus on variability at seasonal and shorter timescales, which the long-term model drift has little impact on.

3. Methods

The various filtered p'_b time series needed for our analyses are obtained as follows for each grid point and each ensemble member. Global mean values are removed every day from each ensemble member following Greatbatch (1994) to account for the lack of mass conservation in the model. Subseasonal time series, containing periods <60 days, are computed by removing the 30-day running mean from daily p'_b time series. This filtering method also partly reduces signals with period $T < 60$ days (by a factor of $\text{sinc}(\pi \frac{30}{T})$, which is 0.64 for $T = 60$ days, reducing to 0 at $T = 30$ days, and <0.25 at $T < 30$ days), but most subseasonal variability is kept and we do not expect major differences in our results from using other high-pass filters. We use the moving-average filter here for its simplicity and computational efficiency. The mean seasonal cycle and intra-annual p'_b series are calculated as follows. Daily p'_b are first averaged in each month to arrive at time series of 252 months (i.e., 21 years). The monthly p'_b values for each particular month, from January to December, are averaged over all 21 years to obtain the mean seasonal cycle. Intra-annual p'_b time series are obtained by removing the mean seasonal cycle and the 12-month running mean from the monthly p'_b fields.

Over each frequency band, we then separately quantify amplitudes of p_b^f and p_b^i . We denote bottom pressure anomalies on a given grid point (x, y) for m th ensemble member as $p'_b(x, y, t, m)$, in which m ranges from 1 to 50, and t represents days (or months) from 1995 to 2015. Following Leroux et al. (2018), $p'_b(x, y, t, m)$ consists of externally forced and intrinsic signals, that is, $p'_b(x, y, t, m) = p_b^f(x, y, t) + p_b^i(x, y, t, m)$, in which $p_b^f(x, y, t) = \langle p'_b(x, y, t, m) \rangle$, where $\langle \rangle$ is the ensemble-mean operator, with the term representing forced variations which are common to all ensemble members. We note that the ensemble-mean may contain some potential phase-locked intrinsic variability but should largely reflect forced signals and has been widely used in such context (e.g., Leroux et al., 2018). The residual term $p_b^i(x, y, t, m)$ indicates the ensemble member dependent pressure variations emerging from the perturbed initial conditions. Note that time-mean values of $p'_b(x, y, t, m)$ are zero, thus time-mean values of both forced and chaotic intrinsic signals, $\overline{p_b^f(x, y, t)}$ and $\overline{p_b^i(x, y, t, m)}$, in which the bar symbol is the time-mean operator, are also zero.

The amplitude of the atmospherically driven pressure variability is quantified as the standard deviation over time domain of the forced pressure time series:

$$\sigma^f(x, y) = \sqrt{\langle [p_b^f(x, y, t)]^2 \rangle}. \quad (1)$$

The amplitude of intrinsic variations is similarly calculated based on the residual time series $p_b^i(x, y, t, m)$. For each time step, we take the square root of the time-averaged variances over the 50 ensemble members. This yields:

$$\sigma^i(x, y) = \sqrt{\langle [p_b^i(x, y, t, m)]^2 \rangle}. \quad (2)$$

We also examine the dependence of results on spatial scales by comparing the statistics above calculated from spatially averaged p_b fields over $3^\circ \times 3^\circ$ (consistent with GRACE and GRACE-FO data resolution) and $10^\circ \times 10^\circ$ cells. After the spatial averaging, mesoscale features are smoothed out, allowing us to infer chaotic intrinsic signatures over larger spatial scales.

4. Results

4.1. Intrinsic Variations in Subseasonal Band

The global map of σ^i (Figure 1a) exhibits highest values (>1.5 cm; all our results are presented in equivalent water column height units with 1 cm \sim 1 hPa) in regions where strong instabilities and intensive eddy generation are observed (e.g., Tulloch et al., 2011), such as the Argentine Basin, along the path of the Antarctic Circumpolar Current (ACC), the Agulhas Current, the Kuroshio and the Gulf Stream and their extensions. Most basin interiors, in contrast, show very weak σ^i (<0.2 cm), as expected from the relative lack of mesoscale instabilities. One exception is the eastern tropical Pacific, where σ^i can be up to 0.7 cm. The relatively stronger σ^i in these regions could be associated with eddy energy radiating from tropical instability waves (e.g., Farrar, 2011; Willett et al., 2006) or from the eastern boundary.

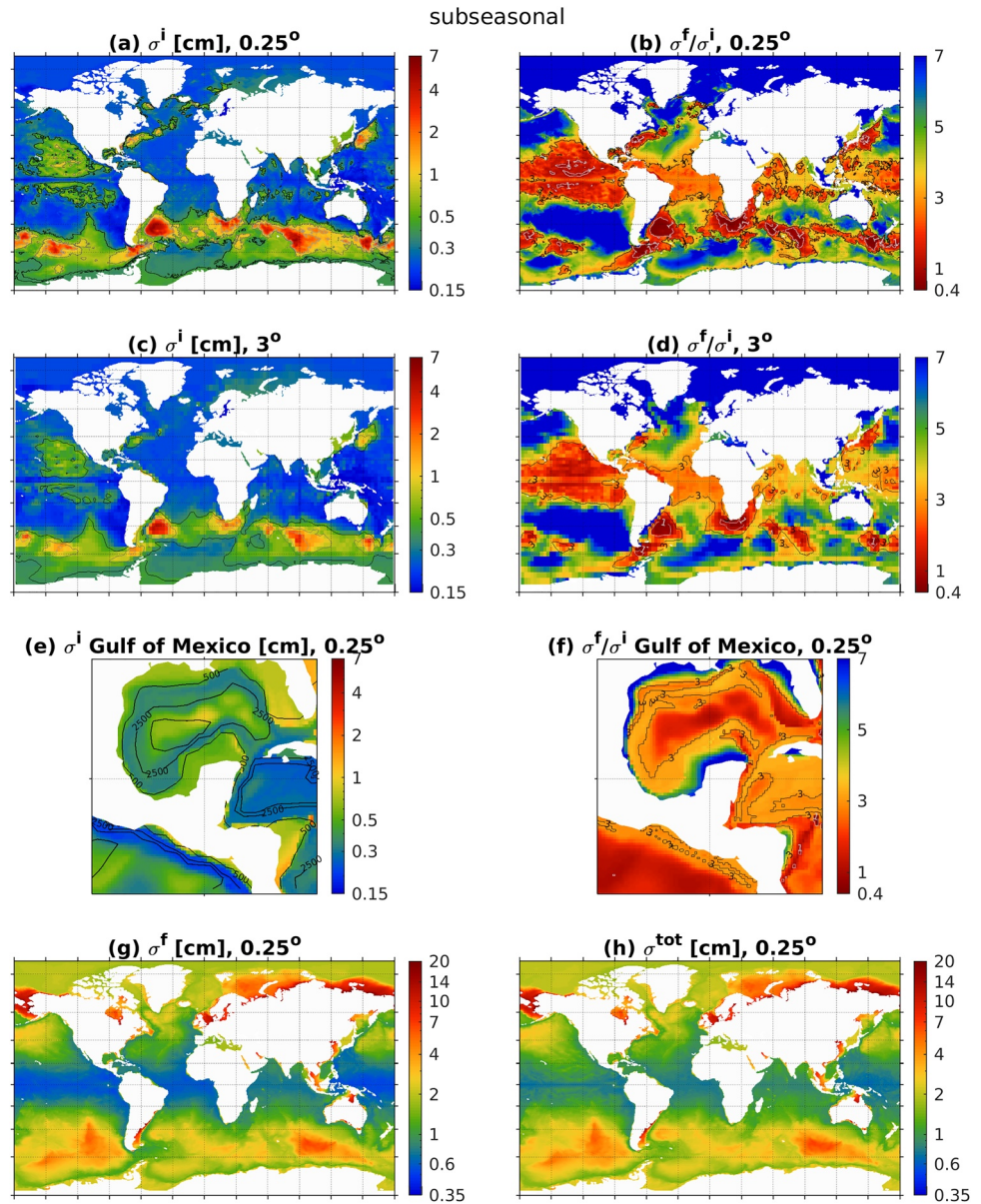


Figure 1. Map of σ^i [cm] (a), (c), (e) and σ^f/σ^i (b), (d), (f) for subseasonal signals (period <60 days) at the original OCCIPUT resolution (a), (b), for smoothed pressure field over $3^\circ \times 3^\circ$ cells (c), (d), and over the Gulf of Mexico (e), (f). Black, dark gray and gray contours in (a) and (c) indicate σ^i values of 0.4, 0.8 and 1.5 cm. Black contours in (e) represent bathymetry of 500, 2500 and 4000 m. Gray and black contours in (b), (d), and (f) indicate the ratio of 1 and 3. Maps of σ^f [cm] (g) and square root of total variances $\sigma^{\text{tot}} = \sqrt{\sigma^f{}^2 + \sigma^i{}^2}$ (h) for subseasonal signals are also shown.

Continental shelf areas also exhibit enhanced σ^i , with amplitude larger than the deep basin interiors by a few millimeters. In some shelf regions, such as Southeast Asia, Southeast North America, South America and Southeast Africa, σ^i can be as large as 1 cm. A closer look at σ^i in the Gulf of Mexico (Figure 1e) suggests regions of high intrinsic variations following the bathymetry. Although the topography may suppress eddies propagating toward the shelf, any sea level signals from baroclinic eddy variability that makes it over the shelves translate into p_b signals, as suggested by the high correlation between sea level and p_b over shallow regions (e.g., Bingham & Hughes, 2008; Vinogradova et al., 2007). The complicated eddy-topography interactions could also lead to the generation of topographic eddies and waves (e.g., Cherian, 2016; Wang, 1992).

To quantify the importance of σ^i relative to σ^f , we examine the ratio σ^f/σ^i (Figure 1b). This ratio can indicate how representative p_b fields are from coarse-resolution models, which strongly underestimate intrinsic variability,

and are often used for GRACE de-aliasing. Low values of σ^i/σ^f suggest that the phase of p_b variations are more “random” (i.e., less correlated with the forcing) and thus less predictable. Regions of low σ^i/σ^f in general follow large σ^f values. In regions of high mesoscale activity and strongest σ^f , intrinsic variations can equal or even overpower forced variations. These oceanic intrinsic processes can play an important role in transporting physical and biological properties such as mass and chlorophyll in the subseasonal band (e.g., Gaube & McGillicuddy, 2017).

Over subtropical and tropical oceans, besides the high σ^f in eastern tropical Pacific, σ^i/σ^f ratios are relatively low, generally <3 , even in basin interiors with small σ^f amplitudes. This is attributed to the low σ^f over these areas (e.g., Quinn & Ponte, 2011), where subseasonal wind and pressure forcing are relatively weak, compared to higher latitudes, and project better on baroclinic motions that tend to have weak p_b signatures (Piecuch et al., 2015). In coastal regions, although σ^i is generally enhanced, σ^f can be quite large, ranging from ~ 5 cm to ~ 20 cm (Figure 1g). This makes the intrinsic variations over coastal regions relatively less important (Figures 1e and 1f).

To further examine the importance of σ^i in contributing to aliasing in the GRACE data, we smooth out the mesoscale features by averaging the OCCIPUT p_b fields within $3^\circ \times 3^\circ$ cells (similar to GRACE data resolution) and re-examine the values of σ^i and the ratios σ^i/σ^f (Figures 1c and 1d). Although appearing to be smoother, both quantities do not show substantial differences from those in Figures 1a and 1b. The results suggest substantial σ^i at scales resolved by GRACE-type observations over lower latitudes and eddy-rich sites, pointing to the potential challenges to accurately de-alias GRACE measurements.

4.2. Intra-Annual Intrinsic Variations

Intrinsic intra-annual p_b signals have a common spatial distribution with subseasonal signals but display overall larger σ^i magnitudes (Figure 2a). Near western boundary currents (WBC) and the ACC, σ^i can be >10 cm. In general, at intra-annual timescales, the contribution of intrinsic processes is substantial almost everywhere, with σ^i amounting to more than a third of σ^f except for the Arctic and the subpolar Pacific, even in regions of weak eddy activity such as the Atlantic basin interior (Figure 2b). Intrinsic variations over almost a quarter of the ocean area (around WBC and ACC) are more important than forced variations (Figure 2b).

The substantial σ^i values for intra-annual timescales can be attributed to two factors. One is that intra-annual is the dominant timescale for mesoscale turbulence and eddy emergence. The other factor is associated with the eddy-driven energy inverse cascade, in which the kinetic energy of mesoscale motions may spontaneously cascade toward longer space and time scales through nonlinear eddy interactions such as clustering or merging (e.g., Arbic et al., 2014, 2012; Dewar, 2003; Sérazin et al., 2018). This implies that the strong intra-annual σ^i signals could be partly fed by the intrinsic variability at higher frequency.

The generation of low-frequency large-scale intrinsic variations via nonlinear energy transfer can be further illustrated via the examination of σ^i calculated from spatially averaged p_b fields (Figures 2c–2f). When computed from p_b fields averaged over $3^\circ \times 3^\circ$, corresponding to the shortest scales resolved by GRACE, σ^i values >1 cm are still seen in wide areas (Figure 2c). The importance of σ^i relative to σ^f is comparable with those based on 0.25° grids (cf. Figures 2b and 2d), suggesting substantial intrinsic signals contained in GRACE measurements.

Considering yet larger scales and smoothing over $10^\circ \times 10^\circ$ cells (Figures 2e and 2f), amplitudes of σ^i weaken significantly, especially over WBC regions and along the ACC. However, the relative importance of σ^i is still substantial: σ^i amounts to more than a third of σ^f over most of the global ocean, including a broad region encompassing the Argentine Basin and Agulhas Current, where $\sigma^i > \sigma^f$. Spontaneously generated by the eddying ocean, remarkable chaotic intrinsic p_b variability is still present at large spatial scales even after mesoscale features are smoothed out.

4.3. Intrinsic Variability and the Seasonal Cycle

The seasonal cycle is one of the main externally forced climate components of ocean variability. It is thus interesting to examine the extent to which intrinsic processes can affect the seasonal cycle. Intrinsic variations in the mean seasonal cycle are weaker compared to the other two bands already discussed, as expected (Figures 3a and 3b). However, regions of high eddy energy still exhibit important σ^i variability, with $\sigma^i/\sigma^f < 3$.

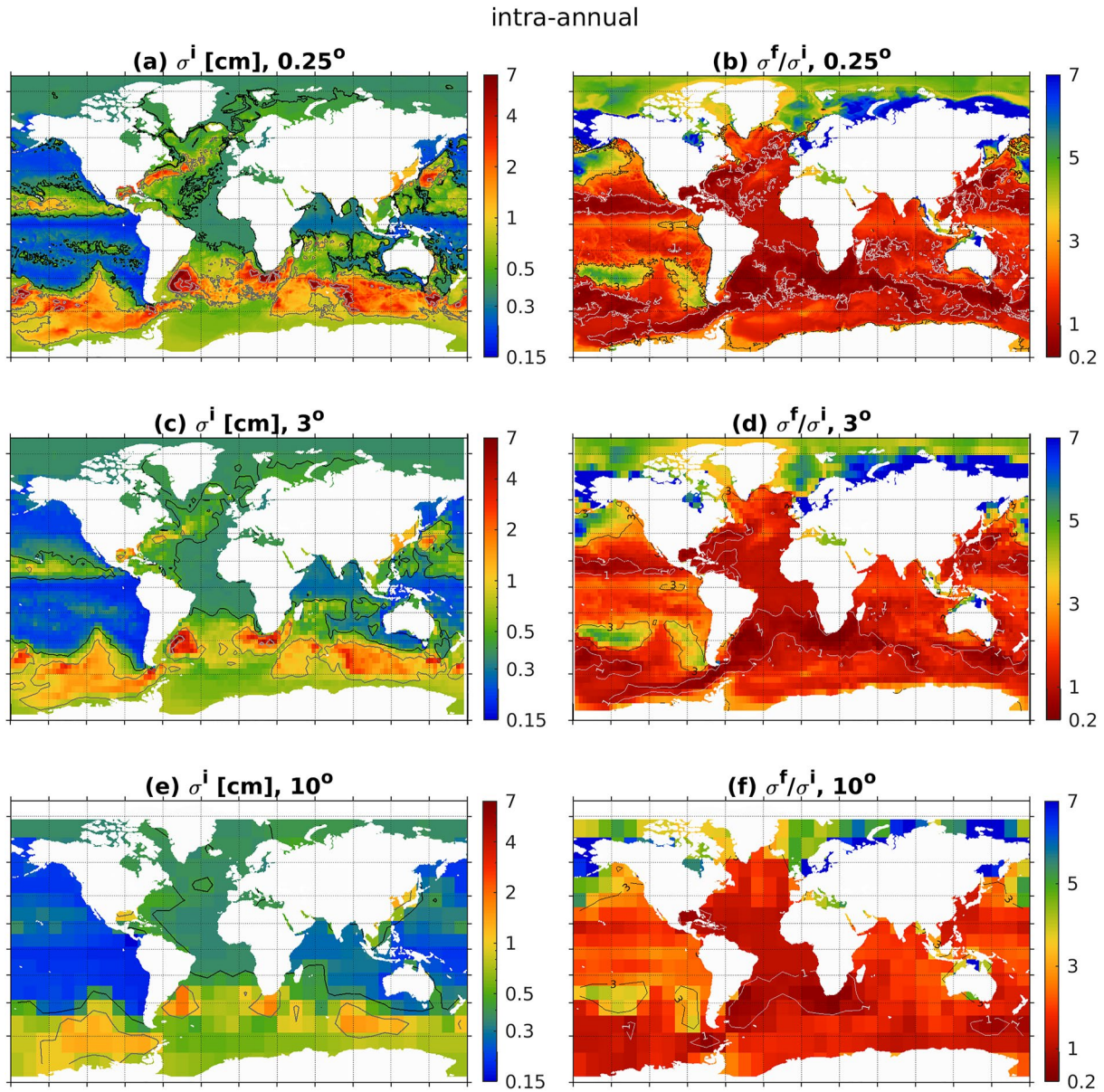


Figure 2. Map of σ^i [cm] (a), (c), (e) and σ^f/σ^i (b), (d), (f) for intra-annual variability at the original OCCIPUT resolution (a), (b), for smoothed pressure field over $3^\circ \times 3^\circ$ cells (c), (d), and over $10^\circ \times 10^\circ$ cells (e), (f). Black, dark gray and gray contours in (a), (c), and (e) indicate σ^i values of 0.4, 1 and 4 cm. Gray and black contours in (b), (d), and (f) indicate the ratio of 1 and 3.

Over regions of higher σ^i , whether intrinsic contributions to the mean seasonal cycle come from changes in amplitude and/or phase can be assessed by examining the mean seasonal cycle for each individual ensemble member. For the examples of the Argentine Basin and Agulhas Current regions (Figures 3c and 3d), based on averaged results over $10^\circ \times 10^\circ$ boxes, mean seasonal cycles show large spread among ensemble members and substantial differences to the forced mean seasonal cycle, in both phase and magnitude. As for the other bands examined, results indicate the impact of intrinsic variability at scales much larger than eddy scales. Other regions of high σ^i (e.g., WBC and ACC, not shown) have consistent patterns with the subseasonal and intra-annual bands.

One might expect eddy generation and related intrinsic variations to be tied to the externally forced mean seasonal cycle itself, leading to potential phase-locking of the forced and intrinsic components. However, eddy nonlinear interactions can lead to phase scrambling and might be behind the large spreads in the mean seasonal cycle among ensemble members. In addition, processes associated with inverse cascade from subseasonal to lower frequencies

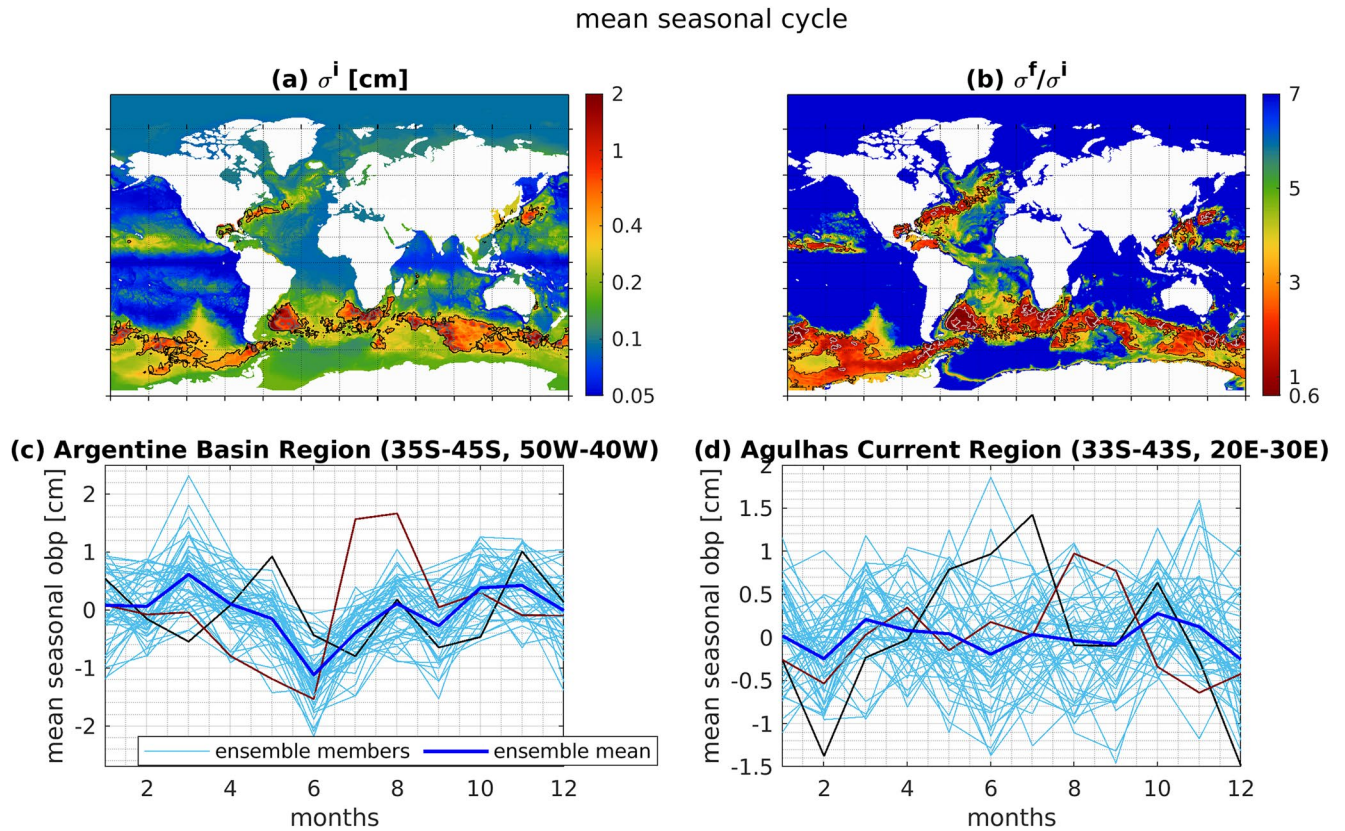


Figure 3. σ^i [cm] (a) and σ^f/σ^i (b) for mean seasonal cycle. Black and gray contours in (a) indicate σ^i values of 0.4 and 1 cm. Gray and black contours in (b) indicate the ratio of 1 and 3. Mean seasonal variations of p_b over Argentine Basin (c) and Agulhas Current (d) from individual ensemble members (light blue lines) and ensemble mean (dark blue lines). Red and black curves in (c) and (d) represent the mean seasonal cycles in two selected ensemble members. All timeseries correspond to spatial mean p_b estimates over the $10^\circ \times 10^\circ$ boxes defined in the titles.

can also contribute to the intrinsic variations detected in the mean seasonal cycle. The weak externally forced mean seasonal p_b variability, together with the presence of intense instabilities, contribute to the lower σ^f/σ^i ratio in these regions.

5. Summary and Discussion

In this paper, we take advantage of p_b output from the eddy-permitting OCCIPUT Large Ensemble to quantify the chaotic intrinsic variations of p_b fields for the mean seasonal cycle, for subseasonal (periods <60 days) and intra-annual (60 days–1 year) bands. Intrinsic variations play a substantial role at all timescales, especially over the intra-annual band, in which $\sigma^i > \sigma^f$ in almost 25% of the global ocean area. The spatial distribution of σ^i is consistent over various frequency bands; strongest σ^i values are present in regions of intense instabilities and mesoscale processes. For intra-annual timescale, σ^i is noteworthy even in basin interiors where eddy activity is considered to be weak.

Spatial patterns of σ^i we present here are consistent with sea level intrinsic variations described by, for example, Penduff et al. (2011) and Sérazin et al. (2015), although the p_b results show smaller amplitudes and are not done for the same frequency bands. This consistency suggests the imprints of surface fluctuations on p_b fields, even if the phase and magnitudes of surface and bottom pressure signals can be different because of the influence of baroclinic processes (e.g., Bingham & Hughes, 2008). Carret et al. (2021) explored the intrinsic variations in steric and manometric components of sea level variability for interannual timescale. As expected, the intrinsic manometric sea level interannual variability has a spatial distribution consistent with our results on p_b for seasonal and shorter timescales, implying a non-negligible intrinsic contribution to the observed p_b and manometric sea level variability across all frequency bands.

Our results have several implications, particularly for processing and interpreting p_b fields from gravity missions like GRACE and GRACE-FO. Notable chaotic intrinsic signals in the subseasonal band reveal the necessity of addressing them in GRACE/GRACE-FO de-aliasing procedures and respective error estimates. De-aliasing with coarse-resolution models is likely to underestimate the subseasonal variations that should be taken out when processing the data from gravity missions. A single run of a fine-resolution model with no data assimilation will not realistically represent intrinsic variations either, as it produces just one chaotic realization of the latter. Estimating intrinsic variability will likely involve eddy-resolving models with data assimilation performed on relatively short (weekly) windows, assuming sufficiently dense altimeter or other observations. Our results provide a crude estimate of the magnitude of the errors made under current methods that do not account for intrinsic variations.

Another implication regards the interpretation of the nominal monthly GRACE/GRACE-FO p_b data, which aside from forced signals can also contain a significant intrinsic component (e.g., Hughes et al., 2016), as our results suggest. Thus, differences between these observations and coarse-resolution models, which mostly simulate forced signals, may also indicate the presence of intrinsic signals in the data, rather than simply issues with the estimates of σ^i . In addition, in optimization procedures that assimilate GRACE and GRACE-FO data in coarse-resolution models, respective data weights need to include representation errors associated with σ^i (e.g., Quinn & Ponte, 2008). Otherwise forcing coarse-resolution models to fit data containing large σ^i will lead to overfitting and devalue such estimates.

Some limitations of our results are worthy of note. First, because of the lack of atmospheric pressure forcing in the OCCIPUT ensemble, the “forced” bottom pressure subseasonal variability should be considered an underestimate. Second, intrinsic variations may also be underestimated to some degree in OCCIPUT. Comparison of sea level fields from OCCIPUT and altimetry suggests weaker modeled variability in mesoscale active regions (Carret et al., 2021). One possible explanation relates to the $\sim 1/4^\circ$ resolution in OCCIPUT, which only partly resolves mesoscale eddies. Sea level chaotic intrinsic variability was found to increase in output with finer resolution of $\sim 1/12^\circ$ (Sérazin et al., 2015). Another possible reason is the absence of air-sea coupling. Atmospheric fluctuations may be driven by sea surface temperature changes originating from intrinsic variations in eddy-rich regions. The lack of such feedback mechanisms could result in underestimated eddy activity in models. In contrast, the absence of direct mesoscale energy removal by the atmosphere (i.e., “eddy killing”) (e.g., Rai et al., 2021; Renault et al., 2016) could lead to an overestimation of modeled eddy activity but may not play a dominant role. Therefore, overcoming these limitations could possibly raise the importance of intrinsic variations in p_b , highlighting the necessity of taking intrinsic variations into account when interpreting large-scale observations, de-aliasing GRACE-like data and making projections of future change using climate models.

Data Availability Statement

Intrinsic and atmospherically driven p_b data used in this study are archived on Zenodo (<https://doi.org/10.5281/zenodo.5527127> (Zhao et al., 2021)).

References

- Androsov, A., Boebel, O., Schröter, J., Danilov, S., Macrandar, A., & Ivanciu, I. (2020). Ocean bottom pressure variability: Can it be reliably modeled? *Journal of Geophysical Research: Oceans*, 125(3), e2019JC015469. <https://doi.org/10.1029/2019JC015469>
- Arbic, B. K., Müller, M., Richman, J. G., Shriver, J. F., Morten, A. J., Scott, R. B., et al. (2014). Geostrophic turbulence in the frequency-wavenumber domain: Eddy-driven low-frequency variability. *Journal of Physical Oceanography*, 44(8), 2050–2069. <https://doi.org/10.1175/JPO-D-13-054.1>
- Arbic, B. K., Scott, R. B., Flierl, G. R., Morten, A. J., Richman, J. G., & Shriver, J. F. (2012). Nonlinear cascades of surface oceanic geostrophic kinetic energy in the frequency domain. *Journal of Physical Oceanography*, 42(9), 1577–1600. <https://doi.org/10.1175/JPO-D-11-0151.1>
- Bessières, L., Leroux, S., Brankart, J.-M., Molines, J.-M., Moine, M.-P., Bouttier, P.-A., et al. (2017). Development of a probabilistic ocean modelling system based on NEMO 3.5: Application at eddying resolution. *Geoscientific Model Development*, 10, 1091–1106. <https://doi.org/10.5194/gmd-10-1091-2017>
- Bingham, R. J., & Hughes, C. W. (2008). The relationship between sea-level and bottom pressure variability in an eddy permitting ocean model. *Geophysical Research Letters*, 35(3), L03602. <https://doi.org/10.1029/2007GL032662>
- Carrère, L., & Lyard, F. (2003). Modeling the barotropic response of the global ocean to atmospheric wind and pressure forcing – Comparisons with observations. *Geophysical Research Letters*, 30(6). <https://doi.org/10.1029/2002GL016473>
- Carret, A., Llovel, W., Penduff, T., & Molines, J. M. (2021). Atmospherically forced and chaotic interannual variability of regional sea level and its components over 1993–2015. *Journal of Geophysical Research: Oceans*, 126(4), 1–15. <https://doi.org/10.1029/2020JC017123>
- Charney, J. G. (1971). Geostrophic turbulence. *Journal of the Atmospheric Sciences*, 28(6), 1087–1095. [https://doi.org/10.1175/1520-0469\(1971\)028<1087:g>2.0.co;2](https://doi.org/10.1175/1520-0469(1971)028<1087:g>2.0.co;2)
- Cherian, D. A. (2016). *When an eddy encounters shelf-slope topography* (PhD dissertation). Massachusetts Institute of Technology.

Acknowledgments

This study is funded by NASA through GRACE Follow-On Science Team Grant 80NSSC20K0728 to AER. The OCCIPUT ensemble simulation was achieved using the PRACE Research Infrastructure resource CURIE based in France at TGCC. This work is a contribution to the OCCIPUT and IMHOTEP projects. OCCIPUT has been funded by ANR through contract ANR-13-BS06-0007-01. IMHOTEP is being funded by CNES through the Ocean Surface Topography Science Team (OST/ST). This work is also supported by the French National Programme LEFE (Les Enveloppes Fluides de l’Environnement)—GMMC (Groupe Mission Mercator-Coriolis) by the CRATERE project.

- Close, S., Penduff, T., Speich, S., Molines, J.-M., & Penduff, T. (2021). A means of estimating the intrinsic and atmospherically-forced contributions to sea surface height variability applied to altimetric observations. *Progress in Oceanography*. <https://doi.org/10.1016/j.pocean.2020.102314>
- Cravatte, S., Sérazin, G., Penduff, T., & Menkes, C. (2020). Imprint of chaotic ocean variability on transports in the Southwest Pacific at interannual timescales. *Ocean Science Discussions*. <https://doi.org/10.5194/os-2020-102>
- Dewar, W. K. (2003). Nonlinear midlatitude ocean adjustment. *Journal of Physical Oceanography*, 33(5), 1057–1082. [https://doi.org/10.1175/1520-0485\(2003\)033<1057:nmoa>2.0.co;2](https://doi.org/10.1175/1520-0485(2003)033<1057:nmoa>2.0.co;2)
- Dobslaw, H., Bergmann-Wolf, I., Forootan, E., Dahle, C., Mayer-Gürr, T., Kusche, J., & Flechtner, F. (2016). Modeling of present-day atmosphere and ocean non-tidal de-aliasing errors for future gravity mission simulations. *Journal of Geodesy*, 90, 423–436. <https://doi.org/10.1007/s00190-015-0884-3>
- Dussin, R., Barnier, B., Brodeau, L., & Molines, J. M. (2016). *Drakkar forcing set dfs5*. MyOcean Report.
- Farrar, J. T. (2011). Barotropic Rossby waves radiating from tropical instability waves in the Pacific Ocean. *Journal of Physical Oceanography*, 41(6), 1160–1181. <https://doi.org/10.1175/2011JPO4547.1>
- Fu, L.-L. (2007). Interaction of mesoscale variability with large-scale waves in the Argentine Basin. *Journal of Physical Oceanography*, 37(3), 787–793. <https://doi.org/10.1175/jpo2991.1>
- Gaube, P., & Mcgillcuddy, D. J. (2017). The influence of Gulf Stream eddies and meanders on near-surface chlorophyll. *Deep-Sea Research Part I*, 122, 1–16. <https://doi.org/10.1016/j.dsr.2017.02.006>
- Greatbatch, R. J. (1994). A note on the representation of steric sea level in models that conserve volume rather than mass. *Journal of Geophysical Research: Oceans*, 99(C6), 12767–12771. <https://doi.org/10.1029/94jc00847>
- Grégorio, S., Penduff, T., Sérazin, G., Molines, J.-M., Barnier, B., & Hirschi, J. (2015). Intrinsic variability of the Atlantic meridional overturning circulation at interannual-to-multidecadal time scales. *Journal of Physical Oceanography*, 45(7), 1929–1946. <https://doi.org/10.1175/jpo-d-14-0163.1>
- Gregory, J. M., Griffies, S. M., Hughes, C. W., Lowe, J. A., Church, J. A., Fukumori, I., et al. (2019). Concepts and terminology for sea level: Mean, variability and change, both local and global. *Surveys in Geophysics 2019*, 40(6), 1251–1289. <https://doi.org/10.1007/S10712-019-09525-Z>
- Hughes, C. W., Williams, J., Blaker, A., Coward, A., & Stepanov, V. (2018). A window on the deep ocean: The special value of ocean bottom pressure for monitoring the large-scale, deep-ocean circulation. *Progress in Oceanography*, 161, 19–46. <https://doi.org/10.1016/j.pocean.2018.01.011>
- Hughes, C. W., Williams, J., Hibbert, A., Boening, C., & Oram, J. (2016). A Rossby whistle: A resonant basin mode observed in the Caribbean Sea. *Geophysical Research Letters*, 43(13), 7036–7043. <https://doi.org/10.1002/2016gl069573>
- Johnson, G. C., & Chambers, D. P. (2013). Ocean bottom pressure seasonal cycles and decadal trends from GRACE Release-05: Ocean circulation implications. *Journal of Geophysical Research: Oceans*, 118(9), 4228–4240. <https://doi.org/10.1002/jgrc.20307>
- Landerer, F. W., Wiese, D. N., Bentel, K., Boening, C., & Watkins, M. M. (2015). North Atlantic meridional overturning circulation variations from GRACE ocean bottom pressure anomalies. *Geophysical Research Letters*, 42(19), 8114–8121. <https://doi.org/10.1002/2015GL065730>
- Leroux, S., Penduff, T., Laurent Bessières, J.-M. M., Brankart, J.-M., Sérazin, G., Barnier, B., et al. (2018). Intrinsic and atmospherically forced variability of the AMOC: Insights from a large-ensemble ocean hindcast. *Journal of Climate*, 31(3), 1183–1203. <https://doi.org/10.1175/JCLI-D-17-0168.1>
- Llovel, W., Penduff, T., Meyssignac, B., Molines, J., Terray, L., Bessières, L., & Barnier, B. (2018). Contributions of atmospheric forcing and chaotic ocean variability to regional sea level trends over 1993–2015. *Geophysical Research Letters*, 45(24), 13405–13413. <https://doi.org/10.1029/2018GL080838>
- Penduff, T., Barnier, B., Terray, L., Bessières, L., Sérazin, G., Gregorio, S., & Brasseur, P. (2014). Ensembles of eddy ocean simulations for climate. *CLIVAR Exchanges*, 19(65), 26–29.
- Penduff, T., Juza, M., Barnier, B., Zika, J., Dewar, W. K., Treguier, A. M., et al. (2011). Sea level expression of intrinsic and forced ocean variabilities at interannual time scales. *Journal of Climate*, 24(21), 5652–5670. <https://doi.org/10.1175/JCLI-D-11-00077.1>
- Penduff, T., Llovel, W., Close, S., Garcia-Gomez, I., & Leroux, S. (2019). Trends of coastal sea level between 1993 and 2015: Imprints of atmospheric forcing and oceanic chaos. *Surveys in Geophysics*, 40(6), 1543–1562. <https://doi.org/10.1007/s10712-019-09571-7>
- Penduff, T., Sérazin, G., Leroux, S., Close, S., Molines, J., Barnier, B., et al. (2018). Chaotic variability of ocean heat content: Climate-relevant features and observational implications. *Oceanography*, 31(2), 63–71. <https://doi.org/10.5670/oceanog.2018.210>
- Piecuch, C. G., Fukumori, I., Ponte, R. M., & Wang, O. (2015). Vertical structure of ocean pressure variations with application to satellite-gravimetric observations. *Journal of Atmospheric and Oceanic Technology*, 32(3), 603–613. <https://doi.org/10.1175/JTECH-D-14-00156.1>
- Piecuch, C. G., Quinn, K. J., & Ponte, R. M. (2013). Satellite-derived interannual ocean bottom pressure variability and its relation to sea level. *Geophysical Research Letters*, 40(12), 3106–3110. <https://doi.org/10.1002/grl.50549>
- Ponte, R. M. (1999). A preliminary model study of the large-scale seasonal cycle in bottom pressure over the global ocean. *Journal of Geophysical Research*, 104(C1), 1289–1300. <https://doi.org/10.1029/1998JC900028>
- Ponte, R. M., & Piecuch, C. G. (2014). Interannual bottom pressure signals in the Australian-Antarctic and Bellingshausen Basins. *Journal of Physical Oceanography*, 44(5), 1456–1465. <https://doi.org/10.1175/JPO-D-13-0223.1>
- Quinn, K. J., & Ponte, R. M. (2008). Estimating weights for the use of time-dependent gravity recovery and climate experiment data in constraining ocean models. *Journal of Geophysical Research*, 113(C12). <https://doi.org/10.1029/2008JC004903>
- Quinn, K. J., & Ponte, R. M. (2011). Estimating high frequency ocean bottom pressure variability. *Geophysical Research Letters*, 38(8), 1. <https://doi.org/10.1029/2010GL046537>
- Rai, S., Hecht, M., Maltrud, M., & Aluie, H. (2021). Scale of oceanic eddy killing by wind from global satellite observations. *Science Advances*, 7, 4920–4927. <https://doi.org/10.1126/sciadv.abf4920>
- Renault, L., Molemaker, M. J., Gula, J., Masson, S., & McWilliams, J. C. (2016). Control and stabilization of the Gulf Stream by oceanic current interaction with the atmosphere. *Journal of Physical Oceanography*, 46(11), 3439–3453. <https://doi.org/10.1175/JPO-D-16-0115.1>
- Schindelegger, M., Harker, A. A., Ponte, R. M., Dobslaw, H., & Salstein, D. A. (2021). Convergence of daily GRACE solutions and models of sub-monthly ocean bottom pressure variability. *Journal of Geophysical Research: Oceans*, 126. <https://doi.org/10.1029/2020jc017031>
- Scott, R. B., & Arbic, B. K. (2007). Spectral energy fluxes in geostrophic turbulence: Implications for ocean energetics. *Journal of Physical Oceanography*, 37(3), 673–688. <https://doi.org/10.1175/JPO3027.1>
- Seo, K. W., Wilson, C. R., Chen, J., & Waliser, D. E. (2008). GRACE's spatial aliasing error. *Geophysical Journal International*, 172(1), 41–48. <https://doi.org/10.1111/j.1365-246X.2007.03611.x>
- Sérazin, G., Penduff, T., Barnier, B., Molines, J.-M., Arbic, B. K., Müller, M., & Terray, L. (2018). Inverse cascades of kinetic energy as a source of intrinsic variability: A global OGCM study. *Journal of Physical Oceanography*, 48(6), 1385–1408. <https://doi.org/10.1175/jpo-d-17-0136.1>

- Sérazin, G., Penduff, T., Grégorio, S., Barnier, B., Molines, J.-M., & Terray, L. (2015). Intrinsic variability of sea level from global ocean simulations: Spatiotemporal scales. *Journal of Climate*, *28*(10), 4279–4292. <https://doi.org/10.1175/jcli-d-14-00554.1>
- Tulloch, R., Marshall, J., Hill, C., & Smith, K. S. (2011). Scales, growth rates, and spectral fluxes of baroclinic instability in the ocean. *Journal of Physical Oceanography*, *41*(6), 1057–1076. <https://doi.org/10.1175/2011JPO4404.1>
- Venaille, A., Vallis, G. K., & Smith, K. S. (2011). Baroclinic turbulence in the ocean: Analysis with primitive equation and quasigeostrophic simulations. *Journal of Physical Oceanography*, *41*(9), 1605–1623. <https://doi.org/10.1175/JPO-D-10-05021.1>
- Vinogradova, N. T., Ponte, R. M., & Stammer, D. (2007). Relation between sea level and bottom pressure and the vertical dependence of oceanic variability. *Geophysical Research Letters*, *34*(3), 1–5. <https://doi.org/10.1029/2006GL028588>
- Wang, X. (1992). *Interaction of an eddy with a continental slope* (PhD dissertation). Woods Hole Oceanographic Institution.
- Willett, C. S., Leben, R. R., & Lavín, M. F. (2006). Eddies and tropical instability waves in the eastern tropical Pacific: A review. *Progress in Oceanography*, *69*(2–4), 218–238. <https://doi.org/10.1016/j.pocean.2006.03.010>
- Zhao, M., Ponte, R., Penduff, T., Close, S., Llovel, W., & Molines, J.-M. (2021). *Imprints of ocean chaotic intrinsic variability on bottom pressure and implications for data and model analyses*. Zenodo. <https://doi.org/10.5281/zenodo.5527127>